Biochemistry

Article

Cite This: *Biochemistry* XXXX, XXX, XXX−XXX

pubs.acs.org/biochemistry

Structural Regulation of a Neurofilament-Inspired Intrinsically Disordered Protein Brush by Multisite Phosphorylation

Ruoxing Lei,[†,‡] Jessica P. Lee,[†,‡] Matthew B. Francis,[†,§] and Sanjay Kumar*[,‡,∥]

[†]Department of Chemistry, [‡]Department of Bioengineering, and [∥]Department of Chemical and Biomolecular Engineering, University of California, Berkeley, California 94720, United States

[§]Materials Sciences Division, Lawrence Berkeley National Laboratory, Berkeley, California 94720, United States

Supporting Information

ABSTRACT: Intrinsically disordered proteins (IDPs) play central roles in numerous cellular processes. While IDP structure and function are often regulated by multisite phosphorylation, the biophysical mechanisms linking these post-translational modifications to IDP structure remain elusive. For example, the intrinsically disordered C-terminal sidearm domain of the neurofilament heavy subunit (NFH-SA) forms a dense brush along axonal NF backbones and is subject to extensive serine phosphorylation. Yet, biophysical insight into the relationship between phosphorylation and structure has been limited by the lack of paradigms in which NF brush conformational responses can be measured in the setting of controlled phosphorylation. Here, we approach this question by immobilizing a recombinant NFH-SA (rNFH-SA) as IDP brushes onto glass, and controllably phosphorylating the sequence *in situ* with mitogen-activated protein kinase 1 (ERK2) preactivated by mitogen-activated protein kinase kinase (MKK). We then monitor brush height changes using atomic force microscopy, which shows that phosphorylation induces significant brush swelling to an extent that strongly depends upon pH and ionic strength, consistent with a mechanism in which phosphorylation regulates brush structure through local electrostatic interactions. Further consistent with this mechanism, the phosphorylated rNFH-SA brush may be dramatically condensed with micromolar concentrations of divalent cations. Phosphorylation-induced height changes are qualitatively reversible via alkaline phosphatase-mediated dephosphorylation. Our study demonstrates that multisite phosphorylation controls NFH-SA structure through modulation of chain electrostatics and points to a general strategy for engineering IDP-based interfaces that can be reversibly and dynamically modulated by enzymes.

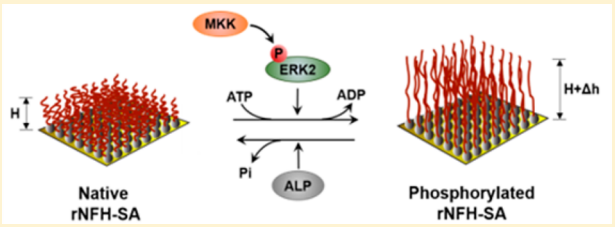

Intrinsically disordered proteins (IDPs) are prevalent in biological systems and regulate several critical cellular processes including cell differentiation, transcription, cell cycle regulation, signaling, and neurogenesis.[1,2] Because IDPs often lack a compact hydrophobic core, they can be highly accessible to post-translational modifications (PTMs),[3] which have been reported to regulate a number of function-driving properties, including structure,[4] protein-binding function,[5] phase transitions,[6] and degradation.[7] Phosphorylation represents the most common type of PTM in IDPs,[1,8] with serine, threonine, and tyrosine phosphorylation all observed to alter IDP structure and protein−protein interactions. Notably, IDPs frequently contain regions that are subject to multisite phosphorylation.[8,9] Regulation of IDP structure by multisite phosphorylation has been explored in a variety of systems,[10−13] revealing a highly complex and context-dependent relationship in which phosphorylation may modulate conformation in either a continuous or discrete, switch-like manner.[4,5]

Importantly, the vast majority of these efforts have characterized IDPs in dilute solution. In many biological contexts, however, IDPs are presented on scaffold-like surfaces, raising the possibility that IDP conformation and phosphosensitivity may be a function of both inter- and intra-IDP interactions. Such IDP arrays, which have been likened to synthetic "polymer brush" coatings, play important roles in controlling transit through nuclear pores, as well as in the structure and mechanics of cytoskeletal networks.[14−16] Neurofilaments (NFs), a key intermediate filament in large myelinated axons, offer a particularly insightful example. NFs run in parallel, cable-like arrays along the length of the axon and play a central role in modulating axon radial growth and caliber.[17] The C-terminal sidearm domains of neurofilament subunits are IDPs that protrude from the rod-like filament backbone and mediate NF−NF spacing by producing a zone of steric exclusion around the NF core.[18,19] In mammals, the NF heavy subunit (NF-H) sidearm domain typically contains 40−60 phosphorylation sites, mostly in the context of lysine-serine-proline (KSP) repeats. NF phosphorylation has been functionally linked to NF assembly, transport, and spacing within the axon,[20,21] and alterations in NF phosphorylation have been

Special Issue: Molecules and the Brain

Received: January 2, 2018
Revised: February 20, 2018
Published: March 20, 2018

DOI: 10.1021/acs.biochem.8b00007
Biochemistry XXXX, XXX, XXX−XXX

associated with a number of neurodegenerative diseases.[22,23] KSP phosphorylation converts the NF-H sequence from a charge-balanced polyampholyte to a polyanion under physiological pH, raising the possibility that phosphorylation may modulate NF conformation through local electrostatic effects. This idea is supported by both computational[24−26] and experimental studies.[19,27,28] Despite the broad consensus around the importance of electrostatic effects in controlling NF sidearm conformation, key mechanistic details remain controversial.[29] For example, it is not clear whether phosphate−phosphate repulsions are sufficient to overcome potential attractive interactions between oppositely charged residues (e.g., lysine and glutamate) on adjacent sidearms.[30] It is also unclear whether the tendency of phosphates to swell the sidearm might be offset by the abundant prolines, which have recently been proposed to structurally "buffer" phosphorylation-driven conformational changes in IDPs.[13]

Part of this controversy may originate from the fact that many mechanistic hypotheses relating NF phosphorylation to structure have been indirectly inferred from studies with assemblies of purified and fully assembled NFs, including reconstituted NF hydrogels.[19,31−33] While phosphorylation-induced network expansion and collapse have been observed in these systems, the response to changes in electrostatic milieu (pH, ionic strength) can be subtle, and the interpretation of the results is confounded to some degree by effects of electrostatics on NF assembly and entanglement, both of which may influence gel structure. As a result, there is a need for paradigms in which NF sidearms (and IDPs in general) can be reconstituted in assemblies that feature intra- and intermolecular interactions, enable phosphorylation, and can be conformationally probed. By analogy, such reconstitution approaches have produced great insight into sequence−structure relationships for synthetic polymers, where expansion and collapse of polymer brushes have been used to decipher molecular regulatory principles.[34,35]

To address this need, we recently developed an experimental IDP brush system in which a recombinant NF-H sidearm domain (rNFH-SA) was surface-immobilized in an oriented fashion and probed with atomic force microscopy (AFM).[36] For the native (i.e., nonphosphorylated) sequence, we observed strongly pH- and ionic strength-dependent conformational transitions, with brush thickness largely correlated with formal charges along the chain. These brushes could be enzymatically modified, with brush height reduced to predictable levels by site-directed proteolysis. To gain further insight into potential effects of phosphorylation, we later created and characterized 32-residue peptide versions of these molecules (containing four KSP repeats) in which we mimicked electrostatic effects of phosphorylation through mutagenesis (KSP to KDP).[37] KDP peptides swelled to a greater degree than KSP peptides, consistent with a model in which phosphate−phosphate repulsion drives conformational properties. However, aspartate replacement may not fully capture electrostatic effects of phosphorylation,[38] and it is challenging to infer conformational properties of the entire NF sequence from such short peptides.

To enable the systematic study of IDP multisite phosphorylation on conformational properties, we now present a system in which an NF-H sidearm may be enzymatically phosphorylated and dephosphorylated in solution and in surface-immobilized brushes. We find that KSP phosphorylation produces a dramatic swelling of the grafted brush and produces pH- and ionic strength-dependent properties characteristic of a strong polyanion. Moreover, phosphorylated brushes may be condensed with micromolar concentrations of divalent cations. By enzymatically phosphorylating the native IDP and probing its conformational changes in a well-defined protein brush system, this work offers a new method to study the effects of multisite phosphorylation events on IDP structure and function. It also provides insight into biophysical mechanisms of NF assembly.

MATERIALS AND METHODS

Plasmid Construction and Expression of rNFH-SA. The IDP expression vector was constructed by modifying the multiple cloning site of pEcoli-Cterm 6×HN vector (Clontech, Cat. No. 631417) to introduce *Eco*RI and *Hin*dIII restriction enzyme recognition sequences, a cysteine near the C-terminus, aromatic residues (to facilitate A280 quantification of the protein), thrombin cleavage site and a 6× histidine tag. The resulting construct was digested with *Eco*RI-HF and *Hin*dIII-HF and subsequently purified. Rat neurofilament heavy protein gene cloned in pCIneo with a *Hin*dIII restriction enzyme site was excised by ApoI and *Hin*dIII-HF digestion. The purified gene insert was then ligated to the doubly digested modified expression vector. Site-directed mutagenesis (QuikChange method adapted from Agilent Technology) was further performed on the resulting modified expression gene to facilitate ribosome binding and to correct the reading frame. For simplicity and consistency with our earlier publication,[36] we term the resulting protein rNFH-SA. However, it should be noted that the construct used in the current study has only one cysteine near the C-terminus, rather than the four N-terminal cysteines of our earlier rNFH-SA. The modified rNFH-SA gene was transformed into 5-α *Escherichia coli* (*E. coli*) cells. Plasmids isolated from the resulting transformants were sequenced, and the encoded amino acid sequence is shown in Figure S1. rNFH-SA was expressed in *E. coli* Rosetta strain (Novagen) as previously described.[36]

Purification of rNFH-SA. The cell pellet was resuspended in lysis buffer [20 mM Tris-HCl (pH 8.0), 300 mM NaCl, 0.07% (v/v) β-mercaptoethanol, 1.5 mM PMSF, and 10 mM imidazole] and lysed by sonic disruption at 4 °C. Insoluble cellular matter was removed by centrifugation, and the supernatant was applied to a HisTrap HP Ni^{2+}-NTA affinity column (GE Healthcare) equilibrated with 10 column volumes of 20 mM Tris-HCl (pH 8.0), 300 mM NaCl, and 10 mM imidazole. The column was then washed with 10 column volumes of wash buffer [20 mM Tris-HCl (pH 8.0), 300 mM NaCl, 34 mM imidazole] and rNFH-SA was eluted with 5 column volumes of elution buffer [20 mM Tris-HCl (pH 8.0), 300 mM NaCl, 250 mM imidazole]. The identity of the eluted protein was verified by SDS-PAGE and LC-MS (ESI-TOF) (6224 TOF and 1200 series HPLC, Agilent Technologies).

Expression and Purification of ERK2. 6× His-tagged wild type rat ERK2 expression plasmid was a generous gift from Dr. Melanie Cobb (UT Southwestern). The plasmid was transformed into the BL21(DE3) competent *E. coli* strain (New England Biolabs), and protein was expressed as previously described.[39] Cells were harvested after 4 h of induction by centrifugation, and then the cell pellet was resuspended in ERK2 lysis buffer [20 mM Tris-HCl (pH 8.0), 300 mM NaCl, 1.5 mM PMSF, and 10 mM imidazole] and lysed by sonic disruption at 4 °C. The clear supernatant obtained from centrifugation was applied to a gravity-flow Ni^{2+}-NTA column equilibrated with 10 column volumes of 20 mM Tris-HCl (pH

DOI: 10.1021/acs.biochem.8b00007
Biochemistry XXXX, XXX, XXX−XXX

8.0), 300 mM NaCl, 10 mM imidazole. The column was washed with 10 column volumes of ERK2 wash buffer [20 mM Tris-HCl (pH 8.0), 300 mM NaCl, 34 mM imidazole], and ERK2 was eluted using a total of 10 column volumes of elution buffer [20 mM Tris-HCl (pH 8.0), 300 mM NaCl, imidazole concentration increasing from 50 to 400 mM].

Expression and Purification of MKK. 6× His-tagged human MKK expression plasmid was a generous gift from the laboratory of Dr. Natalie Ahn (U. Colorado). This variant contains substitutions to phosphorylation sites (S218D, S222D) and neighboring residues (M219D, N221D) and the deletion of residues 44−51 (DN4).[40] The expression and purification methods were modified from Veeranna et al.[41] Specifically, the MKK plasmid was transformed to BL21(DE3) pLysS *E. coli* strain (Promega). Cultures were grown at 30 °C to an optical density at 600 nm of 0.6. IPTG was added to a final concentration of 0.1 mM to induce expression and cells were harvested 12−16 h after induction. To purify MKK, cells were lysed in MKK lysis buffer [50 mM potassium phosphate (pH 8.0), 10% (v/v) glycerol, 0.25% (v/v) Tween-20, 300 mM NaCl] with 1 mM DTT, 1.5 mM PMSF, and 2 mM benzamidine. The cell lysate was sonicated and centrifuged to remove insoluble cell debris before loading to the HisTrap HP column equilibrated with 10 column volumes of MKK lysis buffer with 10 mM imidazole. The column was then washed with 10 column volumes of MKK lysis buffer with 20 mM imidazole and 5 column volumes with 50 mM imidazole. MKK was eluted in lysis buffer with 150 mM imidazole.

Phosphorylation and Dephosphorylation of rNFH-SA in Solution. The phosphorylation protocol was adapted from that of Veeranna et al.[41] First, 1.5 μg of ERK2 was incubated with 0.25 μg of MKK in 20 mM Tris-HCl (pH 7.4) and 50 μM MgATP for 2 h at 30 °C. The reaction mix was then incubated with 10 μg rNFH-SA for 14−16 h at room temperature in 25 mM Tris-HCl (pH 7.4), 2.5 mM $MgCl_2$, 0.05 μM okadaic acid, 0.5 mM EDTA, 0.5 mM EGTA, and 0.5 mM DTT. A final concentration of 0.125−4 mM MgATP was added to achieve various phosphorylation ratios in a total reaction volume of 50 μL. To dephosphorylate rNFH-SA, a final concentration of 0.5 U/μL of calf intestine alkaline phosphatase (ALP, New England Biolabs) was used to incubate with an aliquot of the reaction mixture at 37 °C for 2 h. Phosphorylated and dephosphorylated samples were analyzed by SDS-PAGE stained with either ProQ Diamond phosphorylation gel stain (Thermo Fisher Scientific) for phosphoprotein-specific staining, or Coomassie Brilliant Blue R-250 (BioRad Laboratories). MS data of phosphorylated rNFH-SA were collected in the same way as native rNFH-SA.

In-Gel Digestion of Phosphorylated rNFH-SA. Upon separation by SDS-PAGE and staining with Coomassie Blue, protein bands were excised from the gels and subject directly to tryptic digest. Tryptic digest was performed according to standard procedures[42] with modifications. Briefly, the gel pieces were dehydrated with acetonitrile (ACN, Fisher Scientific) and then rehydrated with 12.5 ng/μL Pierce Trypsin Protease (Thermo Fisher Scientific) in 25 mM NH_4HCO_3 buffer and incubated for 2 h at 37 °C. Peptides were extracted with 50% ACN, 45% H_2O, and 5% formic acid, and concentrated in a vacuum centrifuge. The samples were further analyzed by liquid chromatography-tandem mass spectrometry (LC-MS/MS) using a Dionex UltiMate 3000 RSLCnano LC system that was connected in line with an LTQ-Orbitrap-XL mass spectrometer equipped with an electrospray ionization (ESI) source (Thermo Fisher Scientific; QB3/Chemistry Mass Spectrometry Facility, UC Berkeley). Data analysis to identify tryptic peptides and phosphorylation sites was performed using Proteome Discoverer software (version 1.3, Thermo).

***In Situ* Phosphorylation and Dephosphorylation of rNFH-SA Immobilized Brushes.** Functionalization of borosilicate glass coverslips (Fisherbrand Cover Glasses, Fisher Scientific) and rNFH-SA immobilization were performed as previously described.[36] For *in situ* phosphorylation, ERK2 and MKK were applied at ∼14× concentrations relative to values used for phosphorylation in solution. Specifically, for a 20 μL reaction, 8.4 μg of ERK2 and 1.4 μg of MKK were incubated for 2 h at 30 °C in 25 mM Tris-HCl (pH 7.4), 2.5 mM $MgCl_2$, 0.05 μM okadaic acid, 0.5 mM EDTA, 0.5 mM EGTA, 0.5 mM DTT, and 2 mM MgATP. The reaction mixture was then placed between two rNFH-SA immobilized surfaces. An equal volume of reaction mixture without MgATP was used as a negative control. The samples were allowed to react 16−20 h at room temperature and then rinsed with deionized H_2O containing 1 mM EDTA and 1 mM EGTA, and then deionized H_2O adjusted to pH 11. To dephosphorylate the samples, 5 U/μL calf intestine alkaline phosphatase was incubated between two surfaces at 37 °C or room temperature for 16 h, and then rinsed with deionized H_2O containing 1 mM EDTA and 1 mM EGTA, and then deionized H_2O adjusted to pH 11.

Atomic Force Microscopy (AFM). AFM was performed with a Veeco Catalyst Bioscope (Bruker Corporation, Camarillo, California, USA) using MLCT-BIO A cantilevers, with spring constants determined by thermal tuning. The experimental setup was based on our earlier publication[36] and used an open cell arrangement with a wetted tip brought into contact with samples fully submerged in solution. Typically, at least 200 force curves per coverslip were collected over 100 μm × 100 μm with 2048 data points per curve, at a rate of 2.0 Hz. Relative triggers of up to 4 nN were used to minimize tip−surface damage. When exchanging solutions of different conditions, both the sample and tip were rinsed with several milliliters of the new solution prior to a measurement. The brush height was extracted as previously described based on the difference between the piezo positions at initial deflection and at hard contact.[36] All results were qualitatively reproduced across at least three experimental replicates (i.e., independent surfaces).

RESULTS

rNFH-SA Can Be Phosphorylated *in Vitro* by Recombinant ERK2 and MKK in a Controlled and Reversible Manner. In a previous study, we used an engineered recombinant NFH-SA construct containing residues 426−1066 from the rat NF-H sidearm domain with a tetracysteine tag on the N-terminus.[36] For the current study, to facilitate protein purification and mass spectrometry, we used a very similar construct in which we reduced the number of cysteines from four to one and moved this cysteine to the C-terminus (the full protein sequence is shown in Figure S1). This modified construct (hereafter simply referred to as rNFH-SA) contains 50 KSP repeats and a large and nearly equal number of positively charged (Glu and Asp) and negatively charged residues (Lys and Arg), rendering the unmodified sequence polyampholytic (net neutral) at physiological pH.

To investigate how phosphorylation might affect rNFH-SA structure, we first sought to develop an enzymatic strategy in which we could specifically phosphorylate KSP serines with kinases and then reverse this modification with a phosphatase.

DOI: 10.1021/acs.biochem.8b00007
Biochemistry XXXX, XXX, XXX−XXX

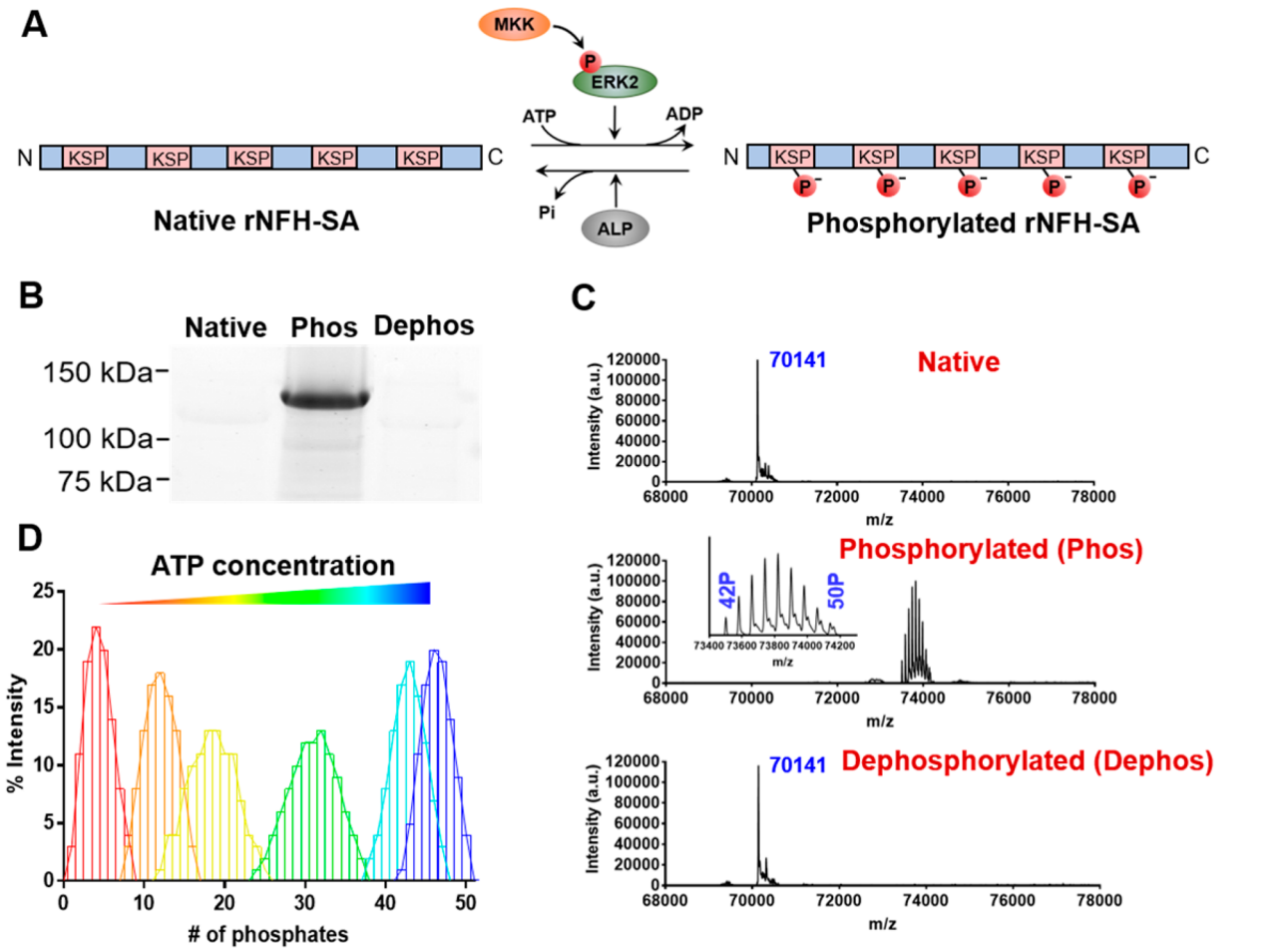

Figure 1. Enzymatic phosphorylation of rNFH-SA. (A) Overview of reactions. rNFH-SA was enzymatically phosphorylated using a two-kinase process involving treatment with ERK2 preactivated with MKK. Dephosphorylation was carried out using alkaline phosphatase (ALP). (B) Phosphoprotein-specific fluorescence staining of SDS-PAGE gels showing phosphorylation and dephosphorylation. The unmodified protein (Native) did not show phosphorylation, whereas kinase treatment (Phos) produced a band at ∼130 kDa, a molecular weight significantly higher than native rNFH-SA with the degree consistent with previous studies.[41] (C) LC/MS analysis. Native rNFH-SA (top) produced a peak at the expected molecular weight of 70141 Da. Kinase treatment (middle) produces a population of peaks spanning a range of 73501−74139 Da, corresponding to the addition of 42−50 phosphates/chain. Treatment with phosphatase (bottom) led to recovery of the native spectrum. (D) Effect of ATP concentration on extent of phosphorylation. Each color histogram represents the LC/MS-determined distribution of phosphospecies over an ATP concentration range of 0.125−4.0 mM. While all ATP concentration produced a heterogeneous distribution of phosphospecies, increasing ATP concentration pushed the distribution to higher average levels of phosphorylation.

The mitogen-activated protein kinase (MAPK) pathway is the major mechanism for the phosphorylation of KSP repeats *in vivo*,[41,43] involving upstream activation of mitogen-activated protein kinase 1 (also known as the extracellular signal-regulated kinase 2, ERK2) by mitogen-activated protein kinase kinase (MAP2K1, or MKK). ERK2/MKK-based phosphorylation has previously been used to phosphorylate purified recombinant NF-H *in vitro* to map phosphorylation sites.[41] Inspired by this strategy, we chose an ERK2/MKK-based system to phosphorylate our rNFH-SA construct (Figure 1A). We expressed rNFH-SA, ERK2, and MKK in *Escherichia coli* and purified both the IDP and the kinases by affinity chromatography (Figures S2−S4).

To validate that ERK2 and MKK may be used to phosphorylate rNFH-SA in solution, we first used MKK to phosphorylate ERK2 in the presence of MgATP, then incubated the reaction mixture with rNFH-SA in phosphorylation buffer overnight (see Materials and Methods). The protein mixture was then analyzed by SDS-PAGE (Figures 1B and S5) and mass spectrometry (Figure 1C). Phosphoprotein-specific fluorescence staining of SDS-PAGE gels showed a strongly positive signal for the kinase-treated reaction mixture (Figure 1B, "Phos"), while native rNFH-SA had a negligible signal (Figure 1B, "Native"). Kinase treatment of rNFH-SA produced an increase in molecular weight on Coomassie-stained gels (Figure S5), consistent with successful phosphorylation. LC-MS analysis of the intact protein further confirmed a molecular weight shift of rNFH-SA after kinase treatment and revealed a nearly normal distribution of phosphorylation stoichiometry. The number of phosphorylated sites scaled with the molar ratio of ATP to rNFH-SA used in the kinase reaction within a certain range, with a ratio of ∼1400:1 (i.e. 28 ATP per KSP repeat) producing an average of ∼46 phosphates/chain and in some cases a maximum of 50 phosphates/chain (Figure 1D). Increasing ATP concentration beyond this point had a marginal impact on the overall extent of phosphorylation (data not shown). Phosphorylation of Ser residues on KSP repeats was further confirmed by MS analysis of the tryptic digested peptide fragments of phosphorylated rNFH-SA (data not shown). We found unique phosphorylated

DOI: 10.1021/acs.biochem.8b00007
Biochemistry XXXX, XXX, XXX−XXX

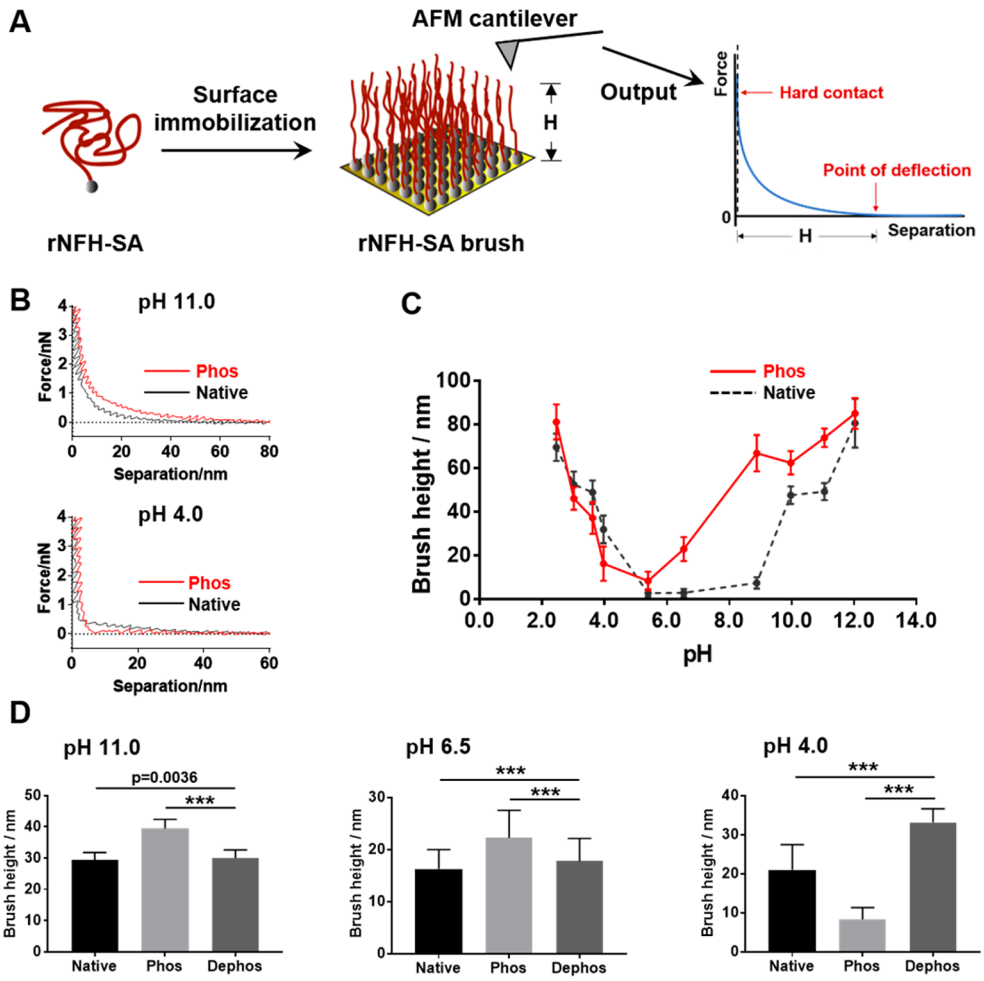

Figure 2. Coordinated regulation of rNFH-SA brush height by phosphorylation and pH. (A) Schematic of rNFH-SA brush assembly and AFM brush height measurement. Brush height was extracted from the tip−sample separation difference between the first point of tip deflection and the hard contact point. (B) Representative AFM force−separation curves for native and phosphorylated brushes at pH 4.0 and 11.0. (C) pH-dependence of phosphorylation-induced swelling of rNFH-SA brushes. In the pH range of 6−12, phosphorylated brushes were more swollen than native brushes, while at pH 3.5 and 4.0 phosphorylated brushes were more condensed. (D) Reversibility of conformational effects by ALP treatment. ***$p < 0.001$, Student's t test with Welch's correction. Error bars represent mean ± SD.

peptides corresponding to each KSP repeat, confirming accessibility of all such repeats to enzymatic phosphorylation. Interestingly, while the majority of phosphorylation occurred on KSP repeats, MS analysis of these peptides also revealed phosphorylation on a few serine or threonine residues other than Ser in KSP repeats (Figure S1, highlighted in green), some of which undergo phosphorylation *in vivo* as well.[44]

To examine if rNFH-SA phosphorylation can be reversed by phosphatase treatment, we further incubated the reaction mixture after phosphorylation with calf intestine alkaline phosphatase (ALP). The resulting mixture was again analyzed by SDS-PAGE and LC-MS. Phosphoprotein-specific fluorescence staining of SDS-PAGE gels showed elimination of the phosphoprotein signal (Figure 1B, "Dephos"), and both Coomassie staining and MS showed reversion of the molecular weight to the native value (Figures S5 and 1C). Thus, enzymatic phosphorylation of rNFH-SA is fully reversible in solution.

Phosphorylation Induces Swelling of rNFH-SA Brushes in a pH-Dependent Manner. We next probed whether phosphorylation influences the conformational properties of grafted layers of rNFH-SA. We immobilized rNFH-SA on maleimide-functionalized silica coverslip surfaces as described previously[36] and phosphorylated the brush *in situ* using more concentrated ERK2 and MKK (14× concentration compared to in-solution phosphorylation assay) to facilitate enzyme penetration to the interior of the brush. We used a "sandwich" assembly for rNFH-SA immobilization as well as phosphorylation to ensure an identical grafting density within the same batch of samples. rNFH-SA surfaces treated with the kinase mixture lacking ATP were used as a negative control. We then utilized AFM to measure forces exerted by the IDP brush layer (Figure 2A). Force curves were acquired within a 100 μm × 100 μm area with separation distances between force measurements chosen to be much larger than the expected interchain spacing distance (estimated to be 7.75 nm based on our previous work).[36] Raw force curves were converted to force−distance curves as previously described,[36] and the brush height was defined as the difference between the scanner position at which the cantilever starts to deflect and the position at which hard contact is achieved. We initially focused on two pH values: pH 11.0, at which the chain is expected to be strongly anionic due to deprotonation of lysines, glutamates, and phosphates; and pH 4.0, at which the chain is expected to

DOI: 10.1021/acs.biochem.8b00007
Biochemistry XXXX, XXX, XXX−XXX

be near polyampholytic due to protonation of both lysine and glutamate as well as incomplete protonation of phosphates. Notably, the effect of phosphorylation on brush thickness depended strongly on pH, with phosphorylation inducing swelling at pH 11 and partial collapse at pH 4 (Figure 2B). To explore this pH regulation further, we compared brush heights for phosphorylated and native brushes over a pH range of 2.5−12, covering nominal pK_a of glutamate (4.1), lysine (10.7), and phosphoserine (pK_{a2}, 5.6). We discovered a similar biphasic trend for both phosphorylated and native IDP brushes (Figure 2C), in which the brush height rises at both ends of the pH curve and reaches a minimum near neutral pH. However, the phosphorylated rNFH-SA brush was significantly more swollen than the native brush from pH 6.5 to pH 12 (Figure 2C), fell to a minimum at pH 4−5, and tracked the native rNFH-SA curve at pH < 3. This phosphorylation-induced difference in pH-dependence is consistent with the idea that phosphorylation converts rNFH-SA from a polyampholyte to a polyelectrolyte, and correspondingly shifts the isoelectric point of the chain.

Phosphorylation-Induced Conformational Changes of rNFH-SA Brushes Are Largely Reversible with Alkaline Phosphatase. We next tested whether enzymatically induced rNFH-SA conformational changes could be reversed by enzymatic dephosphorylation. We performed *in situ* dephosphorylation of the IDP brush using an increased ALP concentration and a prolonged reaction time compared to in-solution dephosphorylation. We then chose three pH values (4.0, 6.5, and 11.0) under which the phosphorylated rNFH-SA brush exhibited distinct heights. As expected, after dephosphorylation, the brush height changes driven by phosphorylation were largely reversed (Figure 2D), consistent with removal of significant numbers of phosphates and strong reversibility of conformational effects.

Both Phosphorylated and Native rNFH-SA Brushes Are Sensitive to Ionic Strength. Ionic strength controls the range and strength of electrostatic interactions and has previously been shown to regulate conformational properties of native NFs.[26,31,45] Our previous study with native rNFH-SA also revealed that brush height is sensitive to ionic strength.[36] Specifically, with the increase of ionic strength, the brush first entered a narrow "osmotic brush regime" in which brush height briefly increased with ionic strength, and then transitioned to a "salted brush regime" in which height fell with subsequent increases in ionic strength. To further explore the ionic strength-sensitivity of phosphorylated brushes, we conducted AFM measurements on both native and phosphorylated brushes at pH 11.0 over a range of NaCl concentrations (Figure 3). We chose pH 11 to render the brush highly anionic, thereby maximizing electrostatic repulsion between the phosphates. Moreover, at pH 11 the native brush is highly swollen, making it easier to detect subtle changes in brush thickness by AFM. We observed a monotonic height decrease of both native and phosphorylated brushes over a range of 2−100 mM NaCl. With 100 mM NaCl, both brush types condensed to <20% of their original heights under the no-salt condition, approaching the sensitivity limit of our measurement (<10 nm). The results are in accordance with the "salted brush" regime in polyelectrolyte theory, in which the negative charges on the protein chains are effectively screened by Na^+ and Cl^-. This similarity in ionic strength sensitivity before and after phosphorylation indicates that both forms of brushes behave like highly charged polymers that can be analyzed using classical polyelectrolyte theory, qualitatively congruent with the mean-field theory of weak polyelectrolyte brushes.[46]

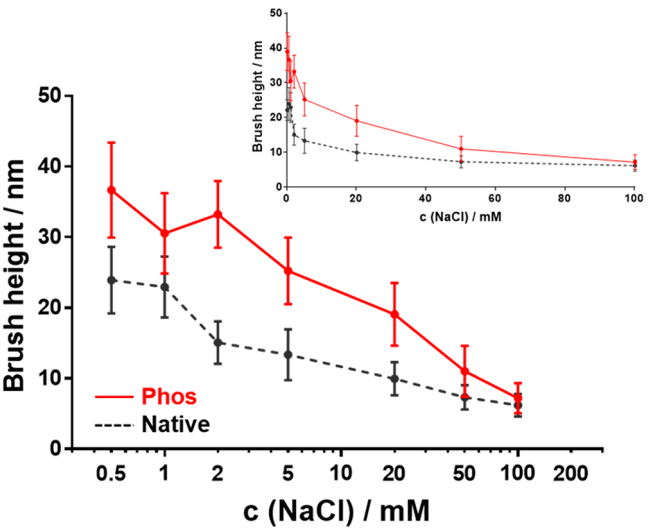

Figure 3. Sensitivity of rNFH-SA brushes to ionic strength before and after phosphorylation. Both native and phosphorylated brushes condensed with increasing NaCl concentration in the range of 2−100 mM at pH 11.0. The inset depicts the same data plotted on a linear scale. Error bars represent mean ± SD.

Phosphorylation Dramatically Enhances rNFH-SA Brush Condensation in Response to Mg^{2+} and Ca^{2+} within Micromolar Concentration. As a final test of the importance of phosphorylation to controlling conformation, we treated the rNFH-SA brush with divalent cations, which are classically observed to condense polyanionic brushes.[47,48] Divalent cations play an especially important role in NF biology, in that intracellular Ca^{2+} has been reported to control NF axonal transport through strongly phosphorylation-dependent cross-bridging interactions.[20,49] On the basis of these findings, we hypothesized that divalent cations such as Ca^{2+} and Mg^{2+} might induce a concerted brush condensation, but only when the brush is polyanionic. Phosphorylation would be expected to support a particularly dramatic effect given the ability of multivalent ions to condense phosphate-based polymers (e.g., DNA).[50] We therefore treated native and phosphorylated rNFH-SA brushes at pH 11.0 over a range of $CaCl_2$ and $MgCl_2$ concentrations and measured brush height by AFM. The average heights of phosphorylated and native brushes at pH 11.0 with no additional salt were used as references ("original height") to quantify the resulting height changes. Treatment with 25 μM $CaCl_2$ reduced the height of the phosphorylated brush by 40% relative to its calcium-free state but had no effect on the height of the native brush. The thickness of the native brush eventually fell for $CaCl_2$ concentrations greater than 50 μM, and then collapsed from ∼85% to ∼40% of the original height from 50 to 100 μM (Figure 4A). A similar trend was observed in the case of $MgCl_2$, in which the phosphorylated brush collapsed by 60% under 100 μM Mg^{2+}, and the native brush collapsed to the same extent under 250 μM Mg^{2+} (Figure 4B). To more precisely define this difference in sensitivity, we also fit the brush height vs divalent cation concentration data (Figure 4A−B) to a four-parameter logistic curve to extract divalent concentrations corresponding to transitions in brush height (Figure S6). For Ca^{2+}, the

DOI: 10.1021/acs.biochem.8b00007
Biochemistry XXXX, XXX, XXX−XXX

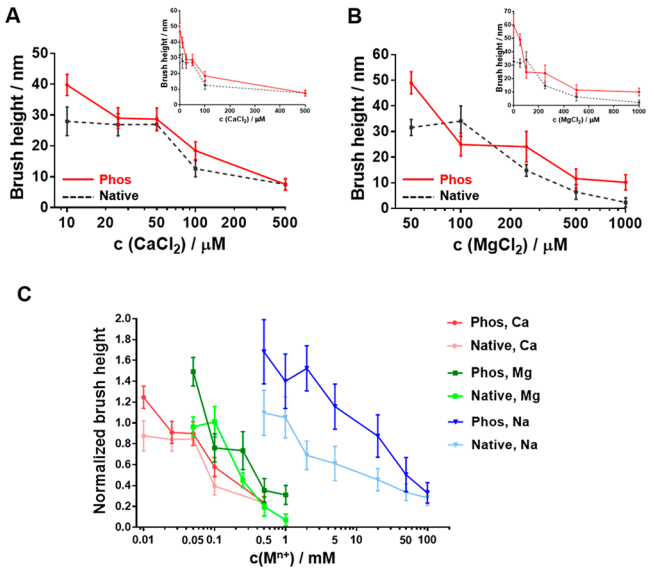

Figure 4. Phosphorylation sensitizes rNFH-SA brushes to divalent cations. At pH 11.0, the phosphorylated rNFH-SA brush began to condense at lower Ca^{2+} (A) and Mg^{2+} concentration (B) than the native brush. The insets depict the same data plotted on linear scales. (C) Summary of all cation responses. Both phosphorylated and native brushes collapsed abruptly in micromolar concentrations of Ca^{2+} or Mg^{2+}, while Na^{+} of the same ionic strength induced only marginal brush condensation. Brush heights are normalized against the average native brush height at pH 11.0, salt-free, from the same experiment, assuming a consistent grafting density. Data for Na^{+} reproduced from Figure 3. Error bars represent mean ± SD.

transition concentration was 75 μM for native rNFH-SA and too small to measure (−520 μM by fit) for phosphorylated rNFH-SA. For Mg^{2+}, the transition concentration was 224 μM for rNFH-SA and 79 μM for phosphorylated rNFH-SA. There was some quantitative variation in this result from sample to sample, which may be a function of imperfect control of grafting density (see Discussion). Nonetheless, the phosphorylation-dependence of brush condensation remained qualitatively consistent in independent replicates. This condensation is much more significant than that would be predicted by purely electrostatic screening effects. For example, both phosphorylated and native IDP brushes exhibited an 80% reduction from the original height under 500 μM of Ca^{2+} or Mg^{2+}, which corresponds to an ionic strength that is approximately equivalent to that of 1.5 mM NaCl predicted by the Debye−Hückel relationship. However, as our studies with NaCl reveal, the heights of both phosphorylated and native brushes fall only modestly (~30%) with 2 mM NaCl. Therefore, this condensation is attributable to cross-linking of phosphates by the multivalent counterions and is consistent with previous reports on polyanion condensation.[47,48] These results underscore the importance of phosphorylation in regulating IDP conformation.

DISCUSSION

Here we report a novel approach to study the effects of multiphosphorylation on NF-H sidearm conformation by enzymatic phosphorylation and dephosphorylation of a surface-immobilized recombinant NF-H sidearm (rNFH-SA) brush. rNFH-SA can be phosphorylated by recombinant ERK2 and MKK and then be reversibly dephosphorylated by ALP *in vitro* on serine residues of multiple KSP repeats. Brush height changes characterized by AFM revealed significant brush swelling after phosphorylation, which is highly dependent on environmental stimuli including pH, ionic strength, and divalent cation concentration (Figure 5). This swelling effect can be attributed

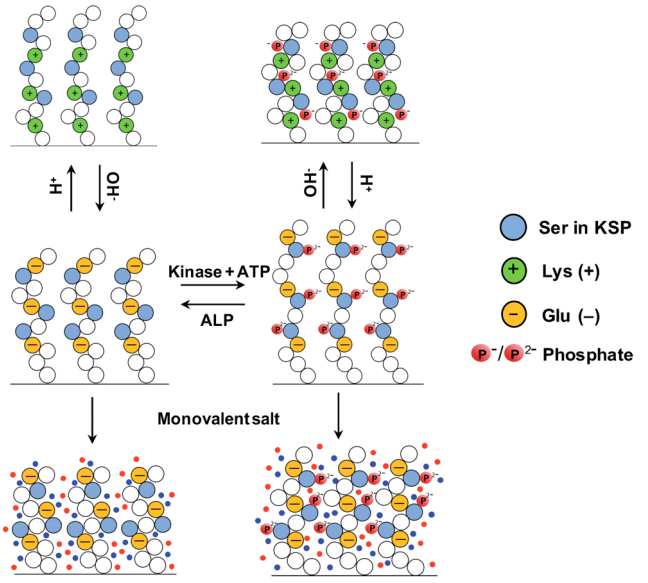

Figure 5. A model illustrating multisite phosphorylation-induced rNFH-SA brush conformational change and its pH- (top) and ionic strength- (bottom) dependence. At basic pH, where phosphate groups are fully deprotonated, phosphorylation of rNFH-SA can induce a significant brush swelling effect and increase brush height, while in weakly acidic solution (e.g., pH 4.0), the addition of phosphate groups introduces attraction between phosphates and protonated lysines, reducing brush height. In the presence of monovalent salt, both native and phosphorylated rNFH-SA brushes condense due to charge screening ("salted brush regime"). Blue and red dots represent monovalent cations and anions, respectively.

to repulsive forces introduced by phosphate groups, which is in agreement with previous computational modeling[25,26] and experimental results,[19,33,51] describing extension of NF sidearms after phosphorylation.

The conformational change of phosphorylated rNFH-SA in response to the electrostatic environment is consistent with observed responses for synthetic polymer brush systems and follows classic polyelectrolyte/polyampholyte theory. The biphasic pH-dependence of brush height for both phosphorylated and native brushes reflects the transition between polyampholyte and polyelectrolyte regimes as dictated by the protein's net charge. Additionally, multisite phosphorylation may shift the isoelectric point (pI) of rNFH-SA to more acidic values, as would be expected given the relative values of the theoretically predicted pI for native rNFH-SA (5.9) and the pK_{a2} of O-phosphoserine (5.6). This is consistent with our pH-dependence measurements (Figure 2C), as the phosphorylated brush reaches maximal condensation at pH 4.0−5.0, whereas the native brush does so at pH 5.0−8.0. Interestingly, brush swelling at basic pH was not observed in our past study on NFH-SA derived phosphomimetic peptide brushes, in which both the native peptide and aspartate-substituted peptide showed a very similar brush height at pH 10.[37] This underscores the idea that phosphomimetic mutations may not fully capture the electrostatic effects of phosphorylation and

DOI: 10.1021/acs.biochem.8b00007
Biochemistry XXXX, XXX, XXX−XXX

that observations with short peptides may not be strictly predictive of full-length IDPs.[38]

Phosphorylated brush conformational sensitivity to ionic strength and divalent cations under basic conditions also aligns with past studies on synthetic polyelectrolytes.[35,47] In the presence of divalent cations, rNFH-SA brushes condense at a much lower ionic strength than is observed for monovalent Na^+, indicating that the divalents are binding and coordinating the phosphates rather than simply screening them. The enhanced sensitivity to divalent counterions upon brush phosphorylation implies a cross-bridging effect, consistent with the hypothesis that Ca^{2+} can promote interfilament association among phosphorylated NFs.[20,52] This similarity to phosphorylated NF sidearms *in vivo* shows the ability of our reconstituted brush system to recapitulate NF sidearm interactions. The structure and physical chemistry of phosphate-bearing polyanion synthetic polymers have not been extensively studied, and our brush paradigm may be useful for gaining new insights into such systems.

It is important to note that the structure and responsiveness of any polymer brush will depend strongly on grafting density, with higher grafting densities amplifying both inter- and intrachain interactions.[34] Whereas grafting densities can be precisely controlled for synthetic polymers by nucleating polymerization at defined densities from a surface (so-called "grafting from" approaches), the use of IDPs necessitated immobilization of already-synthesized chains ("grafting to"). This in turn made it challenging to tightly prescribe grafting density from one sample to another, as reflected in the fact that we observed approximately 2-fold brush height variations across different samples. For this reason, we swept through the full range of each solution condition (e.g., pH) with a single sample and then normalized across samples. To minimize grafting density differences in native- vs phosphorylated- comparisons, we used a "sandwich" assembly to equally expose two entire surfaces to the same reaction mixture so that the IDP should have an equal likelihood of grafting to each surface. Indeed, AFM measurements showed good agreement in brush height for the two halves of the sandwich (data not shown). Conducting the phosphorylation and dephosphorylation reactions *in situ* also guaranteed consistent grafting densities before and after the reactions. However, the number and position of phosphorylated sites may well be different than those measured in solution, making it challenging to map phosphorylation state to brush conformational properties. One way to overcome this limitation in the future would be to use easily reversible grafting chemistries (e.g., disulfides) or introduce an enzymatic cleavage site close to the grafting point so that proteins can be harvested from the surface for further characterization.

The structural consequences of multisite phosphorylation on IDPs have remained largely unpredictable and can vary drastically among different proteins, even with a similar spacing between phosphorylation sites. Recently, elegant work from Martin et al.[13] applied NMR spectroscopy to determine that the conformation of the IDP Ash1 is globally insensitive to phosphorylation due to compensatory responses from adjacent proline residues, despite an average spacing of phosphorylation sites being six residues, a number similar to rNFH-SA. The dramatic expansion of rNFH-SA brushes upon phosphorylation suggests that electrostatic repulsion may overwhelm proline buffering, which may be a consequence of presenting the sequence as a surface-immobilized brush, where inter-IDP interactions contribute strongly to conformational properties. Another intriguing question would be whether surface geometry has an impact on the phosphorylation-induced expansion. Pregent et al.[53] recently immobilized the neurofilament light subunit tail domain on gold nanoparticles and probed for salt-dependent conformational changes. Consistent with our study, these authors observed particle aggregation at high salt concentration and cross-linking by divalent cations. Studies of IDP brush properties on substrates with systematically varying curvatures would add much insight into the role of geometry.

In summary, our study lends both general insight into how multisite phosphorylation modulates the electrostatic properties of IDPs and more specific insight into mechanisms of NF assembly *in vivo*. We anticipate that our enzymatic modification strategies could be applied to other IDP systems in addition to exploring the generality of our findings.

■ ASSOCIATED CONTENT

Supporting Information

The Supporting Information is available free of charge on the ACS Publications website at DOI: 10.1021/acs.biochem.8b00007.

Protein sequence of rNFH-SA; protein purification data of rNFH-SA, ERK2, and MKK; Coomassie Blue stained SDS-PAGE data of rNFH-SA phosphorylation and dephosphorylation; logistic curve-fitting of brush height against divalent cation concentrations (PDF)

■ AUTHOR INFORMATION

Corresponding Author

*Tel (510) 643-0787. Fax (510) 642-5835. E-mail skumar@berkeley.edu.

ORCID

Ruoxing Lei: 0000-0003-3503-174X

Matthew B. Francis: 0000-0003-2837-2538

Author Contributions

R.L. expressed and purified protein samples, prepared surfaces for conjugation, carried out phosphorylation experiments, MS analysis, and AFM measurements. J.P.L. designed the rNFH-SA construct and cloned the plasmid under the joint supervision of S.K. and M.B.F. S.K. raised funds and directed the research. R.L. and S.K. wrote the manuscript. All authors have given approval to the final version of the manuscript.

Funding

The research was supported by grants to S.K. from the NIH (R21EB025017) and the W. M. Keck Foundation.

Notes

The authors declare no competing financial interest.

■ ACKNOWLEDGMENTS

The authors thank the following individuals: Dr. Melaine Cobb and Dr. Natalie Ahn for providing the recombinant ERK2 and MKK plasmids; Anthony T. Iavarone of the QB3/Chemistry Mass Spectrometry for mass spectrometry assistance; Dr. Nithya Srinivasan for guidance on adapting the enzyme purification and phosphorylation/dephosphorylation protocols.

■ ABBREVIATIONS

DTT, 1,4-dithiothreitol; ESI-TOF, electrospray ionization time-of-flight; IPTG, isopropyl β-D-1-thiogalactopyranoside; NTA,

DOI: 10.1021/acs.biochem.8b00007
Biochemistry XXXX, XXX, XXX−XXX

nitrilotriacetic acid; LC-MS, liquid chromatography−mass spectrometry; NMR, nuclear magnetic resonance; PEG, polyethylene glycol; PMSF, phenylmethane sulfonyl fluoride; SDS-PAGE, sodium dodecyl sulfate-polyacrylamide gel electrophoresis

REFERENCES

(1) Dunker, A. K., Bondos, S. E., Huang, F., and Oldfield, C. J. (2015) Intrinsically disordered proteins and multicellular organisms. *Semin. Cell Dev. Biol. 37*, 44−55.

(2) Levine, Z. A., Larini, L., LaPointe, N. E., Feinstein, S. C., and Shea, J.-E. (2015) Regulation and aggregation of intrinsically disordered peptides. *Proc. Natl. Acad. Sci. U. S. A. 112*, 2758−2763.

(3) Theillet, F.-X., Binolfi, A., Frembgen-Kesner, T., Hingorani, K., Sarkar, M., Kyne, C., Li, C., Crowley, P. B., Gierasch, L., Pielak, G. J., Elcock, A. H., Gershenson, A., and Selenko, P. (2014) Physicochemical Properties of Cells and Their Effects on Intrinsically Disordered Proteins (IDPs). *Chem. Rev. 114*, 6661−6714.

(4) Bah, A., Vernon, R. M., Siddiqui, Z., Krzeminski, M., Muhandiram, R., Zhao, C., Sonenberg, N., Kay, L. E., and Forman-Kay, J. D. (2015) Folding of an intrinsically disordered protein by phosphorylation as a regulatory switch. *Nature 519*, 106−109.

(5) Mukhopadhyay, H., de Wet, B., Clemens, L., Maini, P. K., Allard, J., van der Merwe, P. A., and Dushek, O. (2016) Multisite Phosphorylation Modulates the T Cell Receptor ζ-Chain Potency but not the Switchlike Response. *Biophys. J. 110*, 1896−1906.

(6) Brangwynne, C. P., Eckmann, C. R., Courson, D. S., Rybarska, A., Hoege, C., Gharakhani, J., Jülicher, F., and Hyman, A. A. (2009) Germline P Granules Are Liquid Droplets That Localize by Controlled Dissolution/Condensation. *Science 324*, 1729−1732.

(7) Rosenbaum, J. C., Fredrickson, E. K., Oeser, M. L., Garrett-Engele, C. M., Locke, M. N., Richardson, L. A., Nelson, Z. W., Hetrick, E. D., Milac, T. I., Gottschling, D. E., and Gardner, R. G. (2011) Disorder targets misorder in nuclear quality control degradation: a disordered ubiquitin ligase directly recognizes its misfolded substrates. *Mol. Cell 41*, 93−106.

(8) Bah, A., and Forman-Kay, J. D. (2016) Modulation of Intrinsically Disordered Protein Function by Post-translational Modifications. *J. Biol. Chem. 291*, 6696−6705.

(9) Wu, R., Haas, W., Dephoure, N., Huttlin, E. L., Zhai, B., Sowa, M. E., and Gygi, S. P. (2011) A large-scale method to measure absolute protein phosphorylation stoichiometries. *Nat. Methods 8*, 677−683.

(10) Amata, I., Maffei, M., Igea, A., Gay, M., Vilaseca, M., Nebreda, A. R., and Pons, M. (2013) Multi-phosphorylation of the Intrinsically Disordered Unique Domain of c-Src Studied by In-Cell and Real-Time NMR Spectroscopy. *ChemBioChem 14*, 1820−1827.

(11) Kulkarni, P., Jolly, M. K., Jia, D., Mooney, S. M., Bhargava, A., Kagohara, L. T., Chen, Y., Hao, P., He, Y., Veltri, R. W., Grishaev, A., Weninger, K., Levine, H., and Orban, J. (2017) Phosphorylation-induced conformational dynamics in an intrinsically disordered protein and potential role in phenotypic heterogeneity. *Proc. Natl. Acad. Sci. U. S. A. 114*, E2644−E2653.

(12) Liu, B., Chia, D., Csizmok, V., Farber, P., Forman-Kay, J. D., and Gradinaru, C. C. (2014) The Effect of Intrachain Electrostatic Repulsion on Conformational Disorder and Dynamics of the Sic1 Protein. *J. Phys. Chem. B 118*, 4088−4097.

(13) Martin, E. W., Holehouse, A. S., Grace, C. R., Hughes, A., Pappu, R. V., and Mittag, T. (2016) Sequence Determinants of the Conformational Properties of an Intrinsically Disordered Protein Prior to and upon Multisite Phosphorylation. *J. Am. Chem. Soc. 138*, 15323−15335.

(14) Rout, M. P., Aitchison, J. D., Suprapto, A., Hjertaas, K., Zhao, Y., and Chait, B. T. (2000) The Yeast Nuclear Pore Complex: Composition, Architecture, and Transport Mechanism. *J. Cell Biol. 148*, 635−652.

(15) Schoch, R. L., Kapinos, L. E., and Lim, R. Y. H. (2012) Nuclear transport receptor binding avidity triggers a self-healing collapse transition in FG-nucleoporin molecular brushes. *Proc. Natl. Acad. Sci. U. S. A. 109*, 16911−16916.

(16) Janmey, P. A., Leterrier, J.-F., and Herrmann, H. (2003) Assembly and structure of neurofilaments. *Curr. Opin. Colloid Interface Sci. 8*, 40−47.

(17) Yuan, A., Rao, M. V., Veeranna, and Nixon, R. A. (2012) Neurofilaments at a glance. *J. Cell Sci. 125*, 3257−3263.

(18) Brown, H. G., and Hoh, J. H. (1997) Entropic Exclusion by Neurofilament Sidearms: A Mechanism for Maintaining Interfilament Spacing. *Biochemistry 36*, 15035−15040.

(19) Kumar, S., and Hoh, J. H. (2004) Modulation of repulsive forces between neurofilaments by sidearm phosphorylation. *Biochem. Biophys. Res. Commun. 324*, 489−496.

(20) Shea, T. B., and Chan, W. K.-H. (2008) Regulation of neurofilament dynamics by phosphorylation. *Eur. J. Neurosci. 27*, 1893−1901.

(21) Laser-Azogui, A., Kornreich, M., Malka-Gibor, E., and Beck, R. (2015) Neurofilament assembly and function during neuronal development. *Curr. Opin. Cell Biol. 32*, 92−101.

(22) Ackerley, S., Grierson, A. J., Banner, S., Perkinton, M. S., Brownlees, J., Byers, H. L., Ward, M., Thornhill, P., Hussain, K., Waby, J. S., Anderton, B. H., Cooper, J. D., Dingwall, C., Leigh, P. N., Shaw, C. E., and Miller, C. C. J. (2004) p38α stress-activated protein kinase phosphorylates neurofilaments and is associated with neurofilament pathology in amyotrophic lateral sclerosis. *Mol. Cell. Neurosci. 26*, 354−364.

(23) Hu, Y.-Y., He, S.-S., Wang, X.-C., Duan, Q.-H., Khatoon, S., Iqbal, K., Grundke-Iqbal, I., and Wang, J.-Z. (2002) Elevated levels of phosphorylated neurofilament proteins in cerebrospinal fluid of Alzheimer disease patients. *Neurosci. Lett. 320*, 156−160.

(24) Zhulina, E. B., and Leermakers, F. A. M. (2007) Effect of the Ionic Strength and pH on the Equilibrium Structure of a Neurofilament Brush. *Biophys. J. 93*, 1452−1463.

(25) Stevenson, W., Chang, R., and Gebremichael, Y. (2011) Phosphorylation-Mediated Conformational Changes in the Mouse Neurofilament Architecture: Insight from a Neurofilament Brush Model. *J. Mol. Biol. 405*, 1101−1118.

(26) Lee, J., Kim, S., Chang, R., Jayanthi, L., and Gebremichael, Y. (2013) Effects of molecular model, ionic strength, divalent ions, and hydrophobic interaction on human neurofilament conformation. *J. Chem. Phys. 138*, 015103.

(27) Aranda-Espinoza, H., Carl, P., Leterrier, J.-F., Janmey, P., and Discher, D. E. (2002) Domain unfolding in neurofilament sidearms: effects of phosphorylation and ATP. *FEBS Lett. 531*, 397−401.

(28) Lee, S., Sunil, N., and Shea, T. B. (2011) C-terminal neurofilament phosphorylation fosters neurofilament−neurofilament associations that compete with axonal transport. *Cytoskeleton 68*, 8−17.

(29) Shea, T. B., and Lee, S. (2011) Neurofilament phosphorylation regulates axonal transport by an indirect mechanism: A merging of opposing hypotheses. *Cytoskeleton 68*, 589−595.

(30) Jones, J. B., and Safinya, C. R. (2008) Interplay between Liquid Crystalline and Isotropic Gels in Self-Assembled Neurofilament Networks. *Biophys. J. 95*, 823−835.

(31) Rammensee, S., Janmey, P. A., and Bausch, A. R. (2007) Mechanical and structural properties of in vitro neurofilament hydrogels. *Eur. Biophys. J. 36*, 661−668.

(32) Safinya, C. R., Deek, J., Beck, R., Jones, J. B., and Li, Y. (2015) Assembly of Biological Nanostructures: Isotropic and Liquid Crystalline Phases of Neurofilament Hydrogels. *Annu. Rev. Condens. Matter Phys. 6*, 113−136.

(33) Malka-Gibor, E., Kornreich, M., Laser-Azogui, A., Doron, O., Zingerman-Koladko, I., Medalia, O., Beck, R., and Harapin, J. (2017) Phosphorylation-induced mechanical regulation of intrinsically disordered neurofilament protein assemblies. *Biophys. J. 112*, 892−900.

(34) Lego, B., Skene, W. G., and Giasson, S. (2010) Swelling Study of Responsive Polyelectrolyte Brushes Grafted from Mica Substrates: Effect of pH, Salt, and Grafting Density. *Macromolecules 43*, 4384−4393.

DOI: 10.1021/acs.biochem.8b00007
Biochemistry XXXX, XXX, XXX−XXX

(35) Dehghani, E. S., Ramakrishna, S. N., Spencer, N. D., and Benetti, E. M. (2017) Controlled Crosslinking Is a Tool To Precisely Modulate the Nanomechanical and Nanotribological Properties of Polymer Brushes. *Macromolecules 50*, 2932−2941.
(36) Srinivasan, N., Bhagawati, M., Ananthanarayanan, B., and Kumar, S. (2014) Stimuli-sensitive intrinsically disordered protein brushes. *Nat. Commun. 5*, 5145.
(37) Bhagawati, M., Rubashkin, M. G., Lee, J. P., Ananthanarayanan, B., Weaver, V. M., and Kumar, S. (2016) Site-Specific Modulation of Charge Controls the Structure and Stimulus Responsiveness of Intrinsically Disordered Peptide Brushes. *Langmuir 32*, 5990−5996.
(38) Ng, Y.-W., Raghunathan, D., Chan, P. M., Baskaran, Y., Smith, D. J., Lee, C.-H., Verma, C., and Manser, E. (2010) Why an A-Loop Phospho-Mimetic Fails to Activate PAK1: Understanding an Inaccessible Kinase State by Molecular Dynamics Simulations. *Structure 18*, 879−890.
(39) Robbins, D. J., Zhen, E., Owaki, H., Vanderbilt, C. A., Ebert, D., Geppert, T. D., and Cobb, M. H. (1993) Regulation and properties of extracellular signal-regulated protein kinases 1 and 2 in vitro. *J. Biol. Chem. 268*, 5097−5106.
(40) Mansour, S. J., Candia, J. M., Matsuura, J. E., Manning, M. C., and Ahn, N. G. (1996) Interdependent Domains Controlling the Enzymatic Activity of Mitogen-Activated Protein Kinase Kinase 1. *Biochemistry 35*, 15529−15536.
(41) Veeranna, Amin, N. D., Ahn, N. G., Jaffe, H., Winters, C. A., Grant, P., and Pant, H. C. (1998) Mitogen-Activated Protein Kinases (Erk1,2) Phosphorylate Lys-Ser-Pro (KSP) Repeats in Neurofilament Proteins NF-H and NF-M. *J. Neurosci. 18*, 4008−4021.
(42) Shevchenko, A., Tomas, H., Havli, J., Olsen, J. V., and Mann, M. (2007) In-gel digestion for mass spectrometric characterization of proteins and proteomes. *Nat. Protoc. 1*, 2856−2860.
(43) Lee, S., Pant, H. C., and Shea, T. B. (2014) Divergent and convergent roles for kinases and phosphatases in neurofilament dynamics. *J. Cell Sci. 127*, 4064−4077.
(44) Lundby, A., Secher, A., Lage, K., Nordsborg, N. B., Dmytriyev, A., Lundby, C., and Olsen, J. V. (2012) Quantitative maps of protein phosphorylation sites across 14 different rat organs and tissues. *Nat. Commun. 3*, 876.
(45) Beck, R., Deek, J., Choi, M. C., Ikawa, T., Watanabe, O., Frey, E., Pincus, P., and Safinya, C. R. (2010) Unconventional Salt Trend from Soft to Stiff in Single Neurofilament Biopolymer. *Langmuir 26*, 18595−18599.
(46) Pincus, P. (1991) Colloid stabilization with grafted polyelectrolytes. *Macromolecules 24*, 2912−2919.
(47) Yu, J., Mao, J., Yuan, G., Satija, S., Jiang, Z., Chen, W., and Tirrell, M. (2016) Structure of Polyelectrolyte Brushes in the Presence of Multivalent Counterions. *Macromolecules 49*, 5609−5617.
(48) Brettmann, B., Pincus, P., and Tirrell, M. (2017) Lateral Structure Formation in Polyelectrolyte Brushes Induced by Multivalent Ions. *Macromolecules 50*, 1225−1235.
(49) Kushkuley, J., Chan, W. K. H., Lee, S., Eyer, J., Leterrier, J.-F., Letournel, F., and Shea, T. B. (2009) Neurofilament cross-bridging competes with kinesin-dependent association of neurofilaments with microtubules. *J. Cell Sci. 122*, 3579−3586.
(50) Graham, F. L., and van der Eb, A. J. (1973) A new technique for the assay of infectivity of human adenovirus 5 DNA. *Virology 52*, 456−467.
(51) Kumar, S., Yin, X., Trapp, B. D., Hoh, J. H., and Paulaitis, M. E. (2002) Relating Interactions between Neurofilaments to the Structure of Axonal Neurofilament Distributions through Polymer Brush Models. *Biophys. J. 82*, 2360−2372.
(52) Gou, J. P., Gotow, T., Janmey, P. A., and Leterrier, J. F. (1998) Regulation of neurofilament interactionsin vitro by natural and synthetic polypeptides sharing Lys-Ser-Pro sequences with the heavy neurofilament subunit NF-H: Neurofilament crossbridging by antiparallel sidearm overlapping. *Med. Biol. Eng. Comput. 36*, 371−387.
(53) Pregent, S., Lichtenstein, A., Avinery, R., Laser-Azogui, A., Patolsky, F., and Beck, R. (2015) Probing the Interactions of Intrinsically Disordered Proteins Using Nanoparticle Tags. *Nano Lett. 15*, 3080−3087.

DOI: 10.1021/acs.biochem.8b00007
Biochemistry XXXX, XXX, XXX−XXX